Finite element model validation for a 14.5 mm armor piercing bullet impact on a multi-layered add-on armor plate

Adrian Malciu[1,3], *Cristina* Pupăză[2*], *Constantin-Cristinel* Puică[1,4], and *Iuliana-Florina* Pană[4]

[1]Military Equipment and Technologies Research Agency, 16 Aeroportului, Clinceni, Romania
[2]University POLITEHNICA of Bucharest, Robots and Manufacturing Systems Department, 313 Splaiul Independenței Avenue, Bucharest, Romania
[3]University POLITEHNICA of Bucharest, Doctoral School of Industrial Engineering and Robotics, 313 Splaiul Independenței Avenue, Bucharest, Romania
[4]"Ferdinand I" Military Technical Academy, 39-49 George Coșbuc Avenue, Bucharest, Romania

Abstract. For armor plates testing and evaluation the use of modeling and simulation tools, together with a validated finite element model is a reliable approach in respect to a firing conducted session. The paper presents the validation of an advanced finite element model on the impact between two 14,5 mm armor piercing bullets with a multilayered add-on armor plate made by aluminum alloy, alumina tiles, aramid fabric woven, ultra-high molecular weight polyethylene fiber composite and a steel plate. An 8 mm thick armor steel witness plate was placed at 2 cm behind the add-on plate. The real tests were conducted in a firing range and a chronograph was used to measure the values of the bullet impact velocities. The test results showed that the first bullet penetrates the witness plate and the second bullet only deforms it. A three-dimensional finite element model of the bullet and armor plates was conceived to perform the impact simulations in LS-DYNA. Tensile and compression tests, as well as other scientific methods were employed to establish the strength and failure model parameters for each material. The results of the finite element model follow the experimental ones regarding the yaw angle assumptions that were applied for a simulation scenario.

1 Introduction

The equipping of the military vehicles with add-on ballistic protection plates still remains a necessity for its occupants. There are a lot of vehicles that do not combat all the kinetic energy threats only with their basic armor.

In the development process for new and performant armor plates, there are many testing procedures that require real firings against these targets. The employment of real firings comes with some risks for the personnel who conduct the tests and also implies some costs for manufacturing of several target samples required for every scenario or retest cases.

* Corresponding author: cristinapupaza@yahoo.co.uk

© The Authors, published by EDP Sciences. This is an open access article distributed under the terms of the Creative Commons Attribution License 4.0 (http://creativecommons.org/licenses/by/4.0/).

These shortcomings could be mitigated or eliminated by employing modeling and simulation tools as testing or pretesting techniques. The challenges brought by a simulation approach are related to a valid finite element model that is compliant with a real specific scenario and that can be implemented with other future similar scenarios.

First step in this process is to establish the strength and failure models of the materials from which the armor plate and the associated penetrator are built. The most used material for armor application is the high-hardness steel employed in many configurations together with ceramic materials, fiber reinforced composites as aramid fiber woven fabric and ultra-high molecular weight polyethylene fiber (UHMWPE) film [1-4]. These materials can also be used for the blast protection of the civil and industrial infrastructures [5].

In general, the most common strength and failure model in simulation for metallic materials is the Johnson-Cook (J-C) model [6]. The constants of J-C constitutive relation and damage parameters of Johnson-Cook failure model for an armor steel were determined from analysis of experimental data by Banerji et al. in [7]. A comparison between the results obtained from Charpy Impact tests and those obtained from finite element modeling in ABAQUS Explicit software was also presented and a successful prediction of the model parameters was observed. Cao et al. have also presented in [8] that model parameters of J-C constitutive relation for a pipeline steel determined by quasi-static tensile tests, Split-Hopkinson Pressure Bar tests and Charpy impact tests can simulate the failure of the steel under quasi-static and dynamic condition.

Due to the high hardness values, the ceramic materials have an important influence against kinetic energy threats and it is used in many protective structures as helicopter seats, helicopter floor plates, engineering vehicles, armored fighting vehicles and body armor [1]. In the case of an armor system, the ceramic materials are placed on the strike face of the plate [2]. The modeling of the ceramic material subjected to an impact with a solid body is based on several constitutive models. The most used model is that developed by Johnson and Holmquist [1, 9]. The implementation of JH constitutive models in DYNA3D and also the resulted parameters for alumina (Al_2O_3) ceramic are presented in [10]. Those parameters can be also found in [11].

The fiber reinforced composite materials can be met in multi-layered armor plate configurations having a backing function [2]. There are several constitutive models of composite materials for modeling and simulation tools as it can be seen in LS-DYNA software [12]. The implementation of a constitutive model requires specific tensile and compression tests in order to establish the most suitable parameters values in correlation with a finite element model validation for every test that is done. It was found in the literature that some constitutive models for Dyneema HB 26 from DSM [13] or Kevlar from DuPont exist [14].

In this work, a finite element model validation for the impact phenomenon between two 14,5 mm armor piercing bullets with a multi-layered armor plate is presented. In Chapter 2, the multi-layered armor plate and the 14,5 mm armor piercing bullet are described. The experimental setup and results for the two impacts points are also emphasized. The damage level on the armor plate determined by the bullets, the dimension of the crater and also the bulging observed on an 8 mm thick steel witness plate are presented. The methodology of the numerical simulation of the impacts in LS-DYNA software and the obtained results are shown in Chapter 3. Discussions regarding the differences between the experimental results and the numerical simulation ones are outlined taking into consideration the values of the bullet core velocities obtained in the simulation and the ricochet effect of an angled bullet impact. Finally, key findings and general conclusions can be found in Chapter 4.

2 Experimental impact tests and results

2.1 The multi-layered armor plate and the witness plate

The multi-layered armor plate subjected to the two 14,5 mm armor piercing bullets has been realized by sticking together the following layers, as it can be observed in Fig. 1: 2 mm thick aluminum alloy plate, 50×50×10 mm 98% alumina tiles arranged in alternative rows (*a*), 10 mm thick Twaron aramid woven fabric (*b*), 10 mm thick Endumax UHMWPE unidirectional fibers laminated films layer (*c*) and a 3 mm thick armor steel plate (*d*). It was designed to be mounted on the vehicle hull as add-on armor. Consequently, in order to see the benefits of using this add-on armor type, an 8 mm thick witness plate made from high hardness armor steel was placed at 2 cm behind the multi-layered one.

The 2 mm thick aluminum alloy was not represented here, but it was employed on the real armor plate. Moreover, a cover made from aramid woven fabric was applied on every surface of the plate.

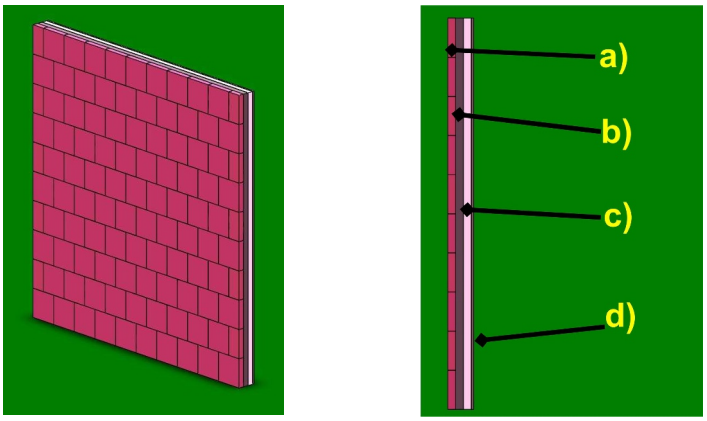

Fig. 1. The multi-layered armor plate (a – isometric view; b – side view).

2.2 The 14,5 mm armor piercing incendiary bullet

The bullet used for experimental research was the armor piercing incendiary bullet from the 14,5×114 mm cartridge, fired with MR4 machine gun. The bullet has a mass of 64 grams and a muzzle velocity at 25 m of 980-995 m/s, according to the manufacturer specifications [15]. The scheme with the bullet components is illustrated in Fig. 2.

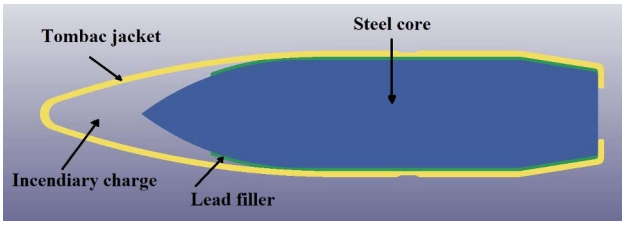

Fig. 2. The 14,5 mm armor piercing incendiary bullet.

2.3 Experimental setup

The armor plate was mounted on its target fixing frame placed at 30 meters distance from the gun muzzle. In order to measure and evaluate the bullet velocities, a chronograph was installed between the gun and the target, at 5 m from the muzzle. The bullets firing was done with MR4 machine gun. The scheme of the experimental setup is presented in Fig. 3.

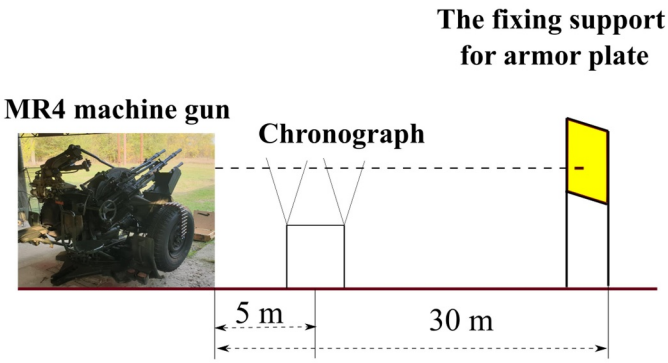

Fig. 3. The experimental setup.

2.4 Experimental results

The impacts of the two bullets on the multi-layered armor plate revealed that the first bullet penetrated the witness plate, but the second did not do it. The recorded values for the impact velocities were 905 m/s for the first bullet, and 910 m/s for the second one.

The resulted diameters of the holes made by the bullets on the steel plate from the back face of the multi-layered armor are presented in Fig. 4.

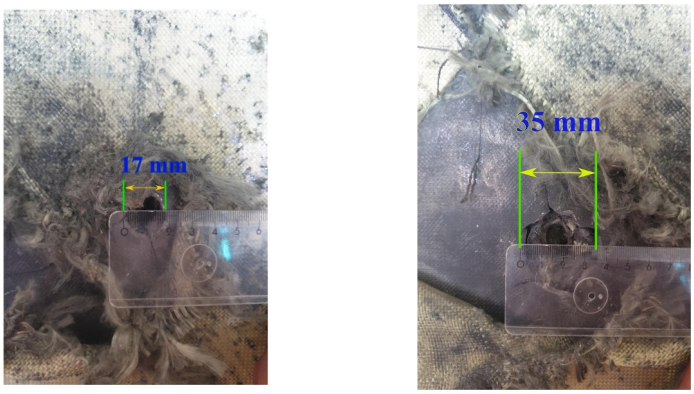

Fig. 4. The diameter of the hole formed in the armor steel layer of the multi-layered plate (left – the first bullet; right – the second bullet).

In the case of the witness plate, for the first impact point, the diameter of the hole after bullet penetration was evaluated to be approximately 14 mm and, for the second point, the

diameter and the height of the bulging area have been measured having 43 mm and 6,8 mm respectively (9,25 mm on the screen minus 2,45 mm, the thickness of the ruler). In Fig. 5 and 6, the ways of how the mentioned parameters were determined are illustrated.

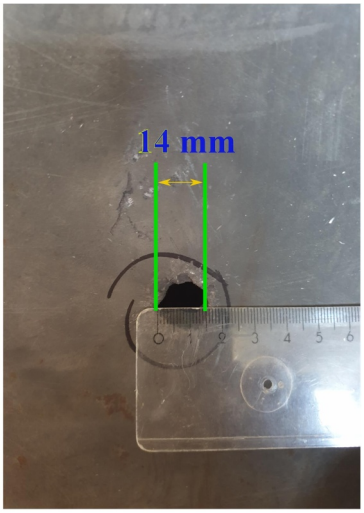

Fig. 5. The hole resulted in the witness plate for the first impact point.

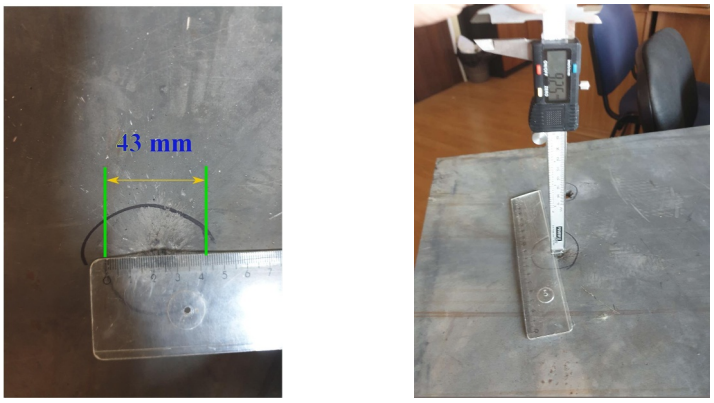

Fig. 6. The diameter of the hole formed in the armor steel layer of the multi-layered plate (left – the first bullet; right – the second bullet).

Behind the witness plate, some sand bags have been put to capture the bullets. After the firing session, the sand bags were examined and no bullet core was found. Therefore, it can be assumed that the high hardness ceramic and also the witness plate have broken the core into fragments.

3 Numerical simulations

The modeling and simulation of the impact phenomenon have been set for two cases: first, when the bullet hits the armor plate perpendicularly, and second having a 1º yaw angle. Because during the firings the bullet with higher impact velocity value did not penetrate the witness plate, the initial velocity of the bullet in the numerical simulations was set to the same value of 905 m/s in order to observe the influence of the yaw angle in the penetration phenomenon.

Because of the high computational time, the three-dimensional model of the multi-layered armor plate has been reduced at the dimensions of an alumina tile, the thickness of each layer remaining the same. The bullet model was built in respect with its real dimensions.

The composite materials were modeled by drawing 10 sublayers with 1 mm thickness for each material. The three-dimensional model is represented in Fig. 7.

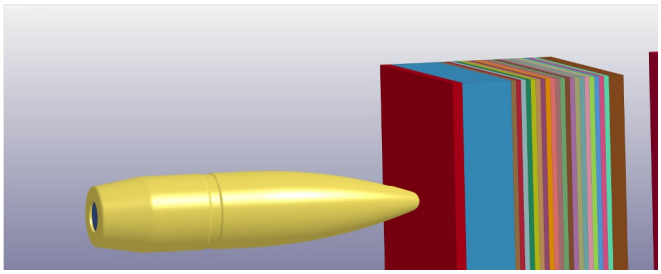

Fig. 7. The three-dimensional CAD model for the bullet, multi-layered armor and witness plate.

3.1 The discretization of the three-dimensional CAD model

After the design process of the three-dimensional models for the armor and bullet in SolidWorks software, they were imported in LS-PrePost (R) V4.7.7 and ICEM-CFD for discretization. A mesh with 1.730.662 hexahedral elements and 4.809.472 nodes has resulted. The elements density can be observed in Fig. 8.

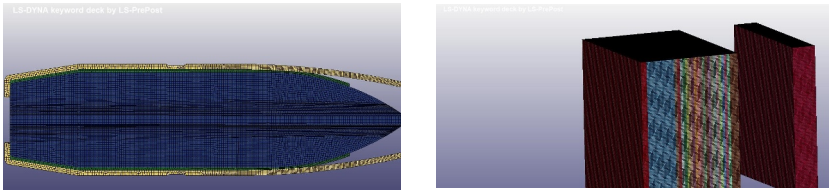

Fig. 8. The discretization level of the three-dimensional model of the bullet and the target components.

3.2 Material models

As it was already mentioned, the choice of the strength and failure models for the materials involved in the simulation is an important step. In this work, for all metallic materials as the core, lead and tombac jacket of the bullet, aluminum plate and also the armor steel plates, the J-C strength and failure model has been applied.

This model expresses the flow stress as a function of effective plastic strain, strain rate and temperature [6, 16, 17]:

$$\sigma_y = \left(A + B\bar{\varepsilon}^{p^n}\right)(1 + C \ln \dot{\varepsilon}^*)\left(1 - T^{*m}\right) \quad (1)$$

$$\dot{\varepsilon}^* = \frac{\dot{\bar{\varepsilon}}^P}{\dot{\varepsilon}_0} \quad (2)$$

$$T^* = \frac{T - T_{room}}{T_{melt} - T_{room}} \quad (3)$$

Where: A=yield strength; B=strengthening constant; C=strain rate constant; n= strengthening exponent; m=thermal softening factor; $\bar{\varepsilon}^{p^n}$=effective plastic strain; $\dot{\bar{\varepsilon}}^P$=strain rate; $\dot{\varepsilon}^*$=dimensional effective strain rate; $\dot{\varepsilon}_0$=reference value for the strain rate; T^*=homologated temperature (dimensionless); T_{room}=room temperature; T_{melt}=melting point; T=current temperature.

The J-C failure model describes the material failure using the following equation [6, 16, 17]:

$$\varepsilon_f = \left(D_1 + D_2 e^{D_3 \sigma^*}\right)(1 + D_4 \ln \dot{\varepsilon}^*)(1 + D_5 T^*), \quad (4)$$

$$\sigma^* = \frac{p}{\sigma_{eff}}, \quad (5)$$

Where: D_1-D_5=failure parameters; σ^*=stress triaxiality factor; p=pressure, σ_{eff}=effective stress.

The failure occurs when the failure parameter reaches a value of unity [6, 16, 17]:

$$D = \sum \frac{\Delta\bar{\varepsilon}^p}{\varepsilon_f} = 1, \quad (6)$$

Where: $\Delta\bar{\varepsilon}^p$=increase in the effective plastic strain value; ε_f=failure strain.

In Table 1, the constants and parameters of the J-C strength and failure model for every material are presented. The room temperature T_{room} was set to 293 K for all the materials involved in the simulation.

Table 1. J-C model constants and parameters.

Parameter	**Bullet steel core** [18]	**Lead jacket** [17]	**Tombac jacket** [17]	**Aluminum plate** [19]	**Armor steel** [20]
ρ [g/cm³]	7,85	11,34	8,96	2,7	7,85
E [GPa]	210	16	124	70	207
ν [-]	0,3	0,42	0,34	0,3	0,33
C_p [J/kgK]	910	-	385	910	450
T_m [K]	1800	-	1356	893	1800
Strength model	*MAT_107	*MAT_098	*MAT_107	*MAT_015	*MAT_015
A [GPa]	1,2	0,024	0,206	0,167	1,58
B [GPa]	50	0,300	0,505	0,596	0,958
n [-]	0,458	1	0,310	0,551	0,175
C [-]	0	0,1	0,025	0,001	0,0087
m [-]	1,0	-	1,09	0,859	0,712
Failure parameters					
D_1	0,051	-	0,540	0,0261	0,068

Parameter	**Bullet steel core** [18]	**Lead jacket** [17]	**Tombac jacket** [17]	**Aluminum plate** [19]	**Armor steel** [20]
D_2	0,018	-	4,88	0,263	5,328
D_3	-3,00	-	-3,03	-0,349	-2,554
D_4	0,0002	-	0,014	0,247	0
D_5	0,55	-	1,12	16,8	0,35
*MAT_ ADD_EROSION	-	VOLEPS=0,5 EPSSH=1	VOLEPS=0,2 EPSSH=1	EFFEPS=2	-

In the case of *MAT_015 material model, an equation of state (EOS) has been required to be defined. Therefore, the Gruneisen equation of state was defined for lead jacket, aluminum plate and armor steel plate material models using *EOS_GRUNEISEN keyword from LS-PrePost [16]. The next constants have been defined: $C=4570$ *m/s*, $S_1=1,49$ and $\gamma_0=1,93$ for steel core [20, 21]; $C=5340$ *m/s*, $S_1=1,4$ and $\gamma_0=1,97$ for aluminum alloy [22].

For the 98% alumina tile, the Johnson-Holmquist JH-2 model [9] has been assigned. This material model is used for brittle materials subjected to large strains, high strain rates and high pressures [9, 16, 17].

Three equations govern the J-H strength model, as follows:

a) for undamaged material:

$$\sigma_i(p,\dot{\varepsilon}) = A_{J-H}\sigma_{HEL}\left(\frac{T-p}{p_{HELL}}\right)^{D_2}\left[1 + C_{J-H}ln\left(\frac{\dot{\varepsilon}}{\dot{\varepsilon_0}}\right)\right], \quad (7)$$

b) for damaged material:

$$\sigma_i(p,\dot{\varepsilon}) = B_{J-H}\sigma_{HEL}\left(\frac{p}{p_{HELL}}\right)^{M_{J-H}}\left[1 + C_{J-H}ln\left(\frac{\dot{\varepsilon}}{\dot{\varepsilon_0}}\right)\right], \quad (8)$$

c) failure model:

$$\varepsilon_p^f(p) = D_1\left(\frac{T-p}{p_{HELL}}\right)^{D_2}, \quad (9)$$

Where: p_{HEL} = pressure for the yield point of Hugoniot; σ_{HEL} = stress for the actual yield point of Hugoniot; A_{J-H} = strength constant of the intact material; N_{J-H}= strength exponent of the intact material; C_{J-H} = strain rate constant; B_{J-H} = strength constant of the damaged material; M_{J-H} = strength constant of the damaged material; D_1 and D_2 = the constant and the exponent of failure respectively [9, 16, 17].

In LS-DYNA PrePost, the *MAT_110 material model is implemented for modeling the ceramic materials. Table 2 provides the 98% purity alumina (Al_2O_3) parameters introduced for the present simulations.

Table 2. The JH-2 model parameter for alumina [17]

Parameter	**Value**
ρ [g/cm^3]	3,84
G [GPa]	93
A [-]	0,93
B [-]	0,31
C [-]	0,007
m [-]	0,6
n [-]	0,64

Parameter	Value
EPSI	1
T [GPa]	0,262
SFMAX [GPa]	1
HEL [GPa]	8
PHEL [GPa]	1,46
Beta	1
D_1 *[-]*	0.01
D_2 *[-]*	0,7
K_1 *[GPa]*	131
K_2 *[GPa]*	0
K_3 *[GPa]*	0
*MAT_ADD_EROSION	VOLEPS=0.05

The modeling and simulation of the composite materials was done by setting the *MAT_022 composite failure model from LS-PrePost. This type of material model uses the next five parameters to compute the matrix cracking, fiber breakage and compression failure criteria: longitudinal tensile strength, transverse tensile strength, shear strength, transverse compressive strength and a nonlinear shear stress parameter. The model is also known as Chang-Chang model [16, 23].

For the aramid woven fabric, the model presented in [24] was applied for the current simulations. The parameters were determined to define the failure model of Twaron CT1000 and they have the next values: Young's modulus in longitudinal direction, *EA=20,44 GPa*; Young's modulus in transverse direction, *EB=8,9 GPa*; Young's modulus in normal direction, *EC=8,9 GPa*; shear modulus in *ab* plane, *Gab=1,64 GPa*; shear modulus in *ac* plane, *Gac=1,64 GPa*; shear modulus in *bc* plane, *Gbc=3,03 GPa*; Poisson's ratio for *ba* plane, v_{ba}*=0,31*; Poisson's ratio for *ca* plane, v_{ca}*=0,31*; Poisson's ratio for *cb* plane, v_{cb}*=0,49*; shear strength, *SC=0,34 GPa*; longitudinal tensile strength, *XT=1,145 GPa*; transverse tensile strength, *YT=0,13 GPa*; transverse compressive strength, *YC=0,65 GPa*, non-linear parameter of shear stress, α*=0* [24].

The UHMWPE uni-directional fiber layer was modeled adapting the parameters found in [25] for Endumax UD tape TA23: Young's modulus in longitudinal direction, *EA=170 GPa*; Young's modulus in transverse direction, *EB=3,8 GPa*; Poisson's ratio for *ba* plane, v_{ba}*=0,346*; Poisson's ratio for *ca* plane, v_{ca}*=0,012*; Poisson's ratio for *cb* plane, v_{cb}*=0,012*; shear strength, *SC=0,02059 GPa*; longitudinal tensile strength, *XT=1,222 GPa*; transverse tensile strength, *YT=0,01438 GPa*; non-linear parameter of shear stress, α*=0*.

3.3 Element formulations and assumptions for contacts and boundaries

The elements formulation for the 20 layers of composite materials was treated by applying the ELFORM=1 option on the *SECTION keyword. For the others materials elements involved in the simulation, ELFORM=2 option has been chosen.

The bullet-armor interaction was performed with the *ERODING_NODES_TO_SURFACE contact option, selecting the bullet nodes and the multi-layered and witness plates parts. In order to simulate the adhesive that sticks together the stratified layers the *AUTOMATIC_SURFACE_TO_SURFACE_TIEBREAK contact option has also been activated for all the surfaces that were in contact at the beginning of the simulation. In addition, the *CONTACT_ERODING_SINGLE_SURFACE has been defined to prevent the over penetration between surfaces from the same body.

The nodes from the lateral surfaces of each layer from the multi-layered armor plate have been fixed with the *BOUNDARY_SET_SPC option to stop its movement in any direction. Additionally, in order to prevent the reflection of the shock waves that can be

generated after the bullet impact, the *BOUNDARY_NON_REFLECTING keyword was also applied on all segments from the same lateral surfaces.

3.4 Results and discussions

The simulations for both scenarios presented above were stopped when the bullet velocity of the first described scenario reached the value of 0 m/s. The simulation with the 1º yaw angle bullet has shown that the velocity values reached a constant evolution at 127 m/s. That has occurred because the elements of the composite layers were eroded from the front of the bullet. In Fig. 9, the final state of deformation is presented for both involved cases.

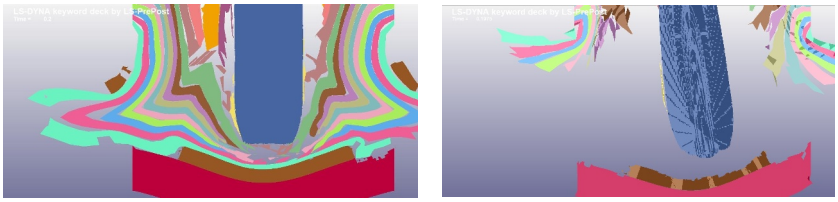

Fig. 9. State of deformation at the termination time of the simulation (left, the bullet with 0º impact angle, and right, the bullet with 1º yaw angle at impact).

As it was previously mentioned, the goal of these two simulations was to observe the influence of the yaw angle regarding perforation capacity of the bullet. In this case, taking into consideration that in both situations the bullet was stopped by the armor, one of the most important parameters to be analyzed remains the bullets velocity evolution during the perforation phenomenon. The plot of the bullets velocity evolution in time is shown in Fig. 10.

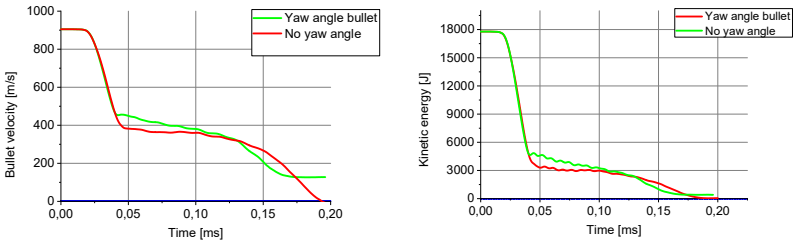

Fig. 10. The bullet core velocity (left) and kinetic energy evolution (right) vs. time.

As it can be observed in Fig. 10, after the bullets passed the alumina layer, the velocity values have been dropped down more rapidly, in the case of the bullet with the 1º yaw angle at impact. This can be explained by the deviations and ricochet effect that were induced to the bullet core especially at its interaction with the alumina tile. Moreover, inducing a ricochet effect to the bullet, a larger contact surface is generated between the bullet and the armor layers and that permits to the next layers to absorb more from the bullet initial kinetic energy. In Fig. 11, the differences between the two bullets regarding the resulted deflection at the time when the simulations were stopped are illustrated.

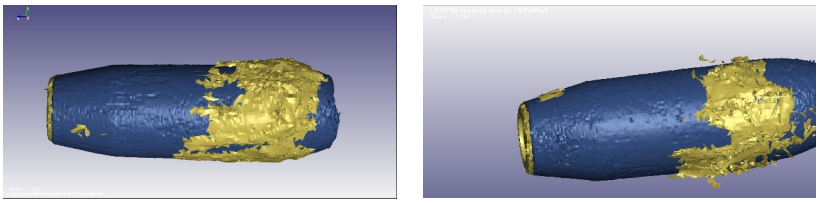

Fig. 11. The effect of the yaw angle against bullet perforation process in YZ plane view (left – no yaw angle, right – the 1º yaw angle, at the t=0,2 ms and t=0,197 ms, respectively).

In the next two pictures from Fig. 12, a comparison regarding the bullet position at the same moment of time is presented in XZ plane section view in order to emphasize the differences between the two impact scenarios. The deformation of the different armor's layers, the hit position of the fragment broken from the 3 mm steel plate and the state of deformation of the bullet can also be seen.

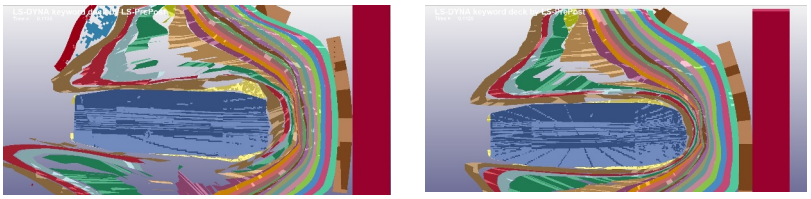

Fig. 12. The state of deformation on at time t=0,1125 ms for both scenarios (left – the normal impact, right - 1º yaw angle impact).

Even if the finite element model has not fulfilled the expectations in regard with the experimental results, some discussions can be done considering the deflection that has been induced to the angled bullet. These could explain why the bullet that has had 910 m/s impact velocity in the firing tests has not perforated the witness plate, because once the bullet has a ricochet a rollover effect can occur. The Fig. 10 also shows that the angled bullet has a longer action on the witness plate and this can be a key finding to understand the bulging occurred in the firing tests and presented in Fig. 6.

4 Conclusions

In this paper experimental research regarding the impact between the 14,5 mm armor piercing incendiary bullet and a multi-layered armor plate has been presented. Two impact cases results, with 905 m/s and 910 m/s bullet impact velocities, have been described. In order to find what is the reason why the bullet with higher impact velocity has not perforated the witness plate, two modeling and simulation scenarios have been defined to see the influence of the yaw angle.

It was found that the modeling and simulation results are in good agreement with the experimental ones regarding the 1º yaw angle assumption. The kinetic energy time evolution for both proposed simulation scenarios showed that when the bullet hits the armor with a yaw angle a kinetic energy decrease occurs. Discussions regarding the experimental tests results vs. modeling and simulations ones were also presented emphasizing the initial kinetic energy differences between both bullets and the kinetic energy loss at the moment when armor steel plate hits the witness plate. Considerations regarding the ricochet effect induced to the angled bullet have explained a possible reason

for the no perforation event that occurred at firing tests in the case of the bullet with the higher velocity.

As such, the use of modeling and simulation as testing or pre-testing techniques can be a reasonable choice, but more attention has to be paid on the materials strength characterization.

In conclusion, future research will focus on better and more reliable predictions. Firstly, tensile and compression specific tests will be conducted to characterize the strength and failure of the materials. After that, the tests results have to be reconsidered in the validation of finite element models that simulate all test conditions until the results match as close as possible the experimental findings. Once the finite element models are validated, the constitutive material models can be used in more complex configurations as the one presented in this work.

This work was supported by a grant of the Ministry of Research, Innovation and Digitization, CNCS/CCCDI – UEFISCDI, project code PN-III-P2-2.1-PED-2019-3997, contract number 402PED/2020, within PNCDI III.

References

1. P. Hazell, *Armour: Materials, Theory, and Design* (CRC Press, 2015)
2. I. Crouch, *The science of armor materials* (Woodhead Publishing, 2016)
3. A. Bhatnagar, *Lightweight ballistic composites: military and law-enforcement applications* (Woodhead Publishing, 2016)
4. X. Chen, *Advanced fibrous composite materials for ballistic protection* (Woodhead Publishing, 2016)
5. N. Uddin, *Blast protection of civil infrastructures and vehicles using composites* (Elsevier, 2010)
6. G. R. Johnson, W. Cook, Eng Fract Mech **21** (1), 31-48 (1985)
7. A. Banerjee, S. Dhar, S. Acharyya, D. Datta, N. Nayak, Mat Sci Engn: A **640**, 200-209 (2015)
8. Y. Cao, Y. Zhen, M. Song, H. Yi, F. Li, X. Li, Int J Mech Sci **179**, 105627 (2020)
9. G. R. Johnson, T. J. Holmquist, *AIP Conf Proc* **309**, 981 (1994)
10. G. A. Gazonas, Army Research Lab Aberdeen Proving Ground, MD - Weapons and materials research directorate (Aberdeen, 2002)
11. D. S. Cronin, K. Bui, C. Kaufmann, G. McIntosh, T. Berstad, *4th European LS-DYNA users conference* **1**, 47-60 (2003)
12. LS-DYNA Keyword user's manual Vol. II, Livermore Software Technology Corporation (2021)
13. DSM. Available on https://www.dsm.com/dyneema/en_GB/home.html .
14. DuPont. Available on https://www.dupont.com/brands/kevlar.html .
15. CN ROMARM SA. Available on : https://romarm.ro/wp-content/uploads/2021/04/27_Datasheet-14.5x114mm-AMMUNITION.pdf .
16. J. Hallquist, *LS-DYNA Theory Manual* (Livermore Software Technology Corporation, 2006)
17. P. Zochowski, M. Bajkowski, R. Grygoruk, M. Magier, W. Burian, D. Pyka, M. Bocian, K. Jamroziak, Mater **15** (1), (2022)
18. D. Mohotti, T. Ngo, P. Mendis, *Numerical simulation of impact and penetration of ogival shaped projectiles through steel plate structures* (2011)
19. A. Rashed, M. Yazdani, A. A. Babaluo, P. Hajizadeh Parvin, J Compos Mater **50** (25), 3561-3576 (2016)
20. N. Kılıç, S. Bedir, A. Erdik, B. Ekici, A. Taşdemirci, M. Güden, Mater Design **63**, 427-438 (2014)
21. T. Niezgoda, A. Morka, World J Eng **1**, 414-417 (2010)
22. H. Ahmed, A. Mubashar, E. Uddin, S. Waheed Ul Haq, Int J Multiphys **15** (2), 119-138 (2021)
23. F. K. Chang, K. Y. Chang, J compos mater **21** (9), 834-855 (1987)
24. S. Feli, M. R. Asgari, Compos Part B- Eng **42** (4), 771-780 (2011)
25. A. Haris, V. B. C. Tan, Int J Impact Eng **151**, 103824 (2021)